



RESEARCH ARTICLE OPEN ACCESS

Intelligent Parameter Identification for a High-Cycle Accumulation Model of Sand With Enhancement of Cuckoo Search Algorithm

Shao-Heng He^{1,2} | Zhen-Yu Yin^{2,3}  | Yifei Sun⁴  | Zhi Ding¹

¹Key Laboratory of Safe Construction and Intelligent Maintenance for Urban Shield Tunnels of Zhejiang Province, Hangzhou City University, Hangzhou, China | ²Department of Civil and Environmental Engineering, The Hong Kong Polytechnic University, Hong Kong, China | ³Research Centre for Resources Engineering towards Carbon Neutrality (RCRE), The Hong Kong Polytechnic University, Hong Kong, China | ⁴Key Laboratory of Ministry of Education for Geomechanics and Embankment Engineering, Hohai University, Nanjing, China

Correspondence: Zhen-Yu Yin (zhenyu.yin@polyu.edu.hk) | Yifei Sun (yifei.sun@hhu.edu.cn)

Received: 16 March 2024 | **Revised:** 25 August 2024 | **Accepted:** 3 September 2024

Funding: This study was supported by Research Grants Council (RGC) of Hong Kong Special Administrative Region Government (HKSARG) of China (Grant No.: 15220221, 15229223, 15227923), Research Centre for Resources Engineering towards Carbon Neutrality (RCRE) of The Hong Kong Polytechnic University (Grant No.: 1-BBEM) and the open fund project of Key Laboratory of Safe Construction and Intelligent Maintenance for Urban Shield Tunnels of Zhejiang Province (Grant No. ZUCC-UST-22-01).

Keywords: constitutive model | high-cyclic loading | optimization algorithm | sand

ABSTRACT

This study presents a novel approach of intelligent parameter identification (IPI) for a high-cycle accumulation (HCA) model of sand, which reduces the subjective errors on manual parameter calibration and makes the use of the HCA model more accessible. The technique is based on optimization theory and adopts the cuckoo search algorithm (CSA). To improve search ability and convergence speed of CSA, several enhancements are implemented. First, the improved CSA (ICSA) incorporates quasi-opposition learning to expand the search space and replaces the original search strategy with a Cauchy random walk to enhance global search ability. Second, an adaptive scaling factor is introduced in the algorithm's control parameters to achieve a better balance between exploration speed and accuracy. Third, a dynamic inertia weight is used to balance the search between global and local spaces when generating new nest positions after abandoning old ones. The performance of the ICSA-based IPI approach is evaluated by comparing it with the original CSA-based IPI and manual calibration in determining the HCA model parameters. A comprehensive analysis is also conducted to assess the effectiveness and superiority of each improvement strategy introduced in the ICSA over the original CSA. All comparisons demonstrate that the proposed ICSA-based IPI method is more powerful and efficient in finding optimal parameters.

1 | Introduction

The long-term serviceability of structures such as railways, water gates, tanks, and offshore foundations is heavily influenced by the residual deformations that occur under high-cyclic loading conditions. High-cyclic loading refers to cyclic loads that involve a large number of cycles ($N \geq 10^3$) with relatively small strain

amplitudes ($\epsilon^{\text{ampl}} \leq 10^{-3}$). Such loading can be caused by various factors, including traffic (e.g., high-speed railways), wind and wave action (e.g., onshore and offshore wind power plants), machine foundations (e.g., gas turbines), or repeated filling and emptying processes (e.g., tanks) [1]. To ensure the long-term functionality of these structures, it is crucial to keep the differential settlements within a very narrow range, especially

This is an open access article under the terms of the [Creative Commons Attribution](https://creativecommons.org/licenses/by/4.0/) License, which permits use, distribution and reproduction in any medium, provided the original work is properly cited.

© 2024 The Author(s). *International Journal for Numerical and Analytical Methods in Geomechanics* published by John Wiley & Sons Ltd.

for structures that are highly sensitive to such settlements. Accurately predicting these deformations becomes essential for ensuring the stability of the infrastructures. To address this, high-cycle accumulation (HCA) models are utilized to forecast the permanent deformations that are generated due to cyclic loading with numerous cycles and small to intermediate strain amplitudes. The literature has proposed various HCA models, including those developed by Pasten et al. [2], Karg et al. [3], Abdelkrim et al. [4], Niemunis et al. [5], and Suiker and de Borst [6]. This study specifically focuses on the HCA model introduced by Niemunis et al. [5], which has been extensively applied in the numerical analysis of ship locks, gas turbines, and offshore wind power plants, as described in Macháček et al. [7], Staubach and Wichtmann [8], and Zachert et al. [9].

A crucial step in utilizing any mathematical model is determining its constants/parameters, commonly known as calibration. The calibration process for the parameters used in the HCA model by Niemunis et al. [5], which quantifies the relationship between strain accumulation rate and strain amplitude, void ratio, average stress, and cyclic preloading, is quite laborious. The complete calibration procedure has been thoroughly described in detail in Wichtmann et al. [10]. It requires conducting several drained high-cyclic triaxial tests with varying stress amplitudes, initial densities, and average stresses. However, their calibration is often time-consuming and demands a high level of expertise in handling the model, as many of the parameters cannot be straightforwardly identified in a single step. As a result, applying such an advanced soil model becomes a highly challenging task not only for beginners but also for experienced engineers and researchers, hindering its practical implementation in projects and boundary value problems. In the past few decades, intelligent parameter identification (IPI) method based on various optimization algorithms (such as genetic algorithm [GA]) has been proposed to simplify and expedite the calibration process [11, 12], particularly reducing the hurdles in using advanced constitutive soil models. IPI not only reduces the workload of manual parameter calibration but also enhances overall efficiency. Furthermore, it can help reduce the reliance on the operator's fitting experience, making it easier for engineers to obtain parameter calibration results. Another advantage of IPI, which may not be immediately apparent, is the ability to identify previously unconsidered interactions among individual parameters and find global optima. Numerous studies have employed IPI methods based on optimization algorithms to calibrate constitutive model parameters. For instance, Pedrosa and Williams [13] proposed an IPI method based on optimization using GA for determining the coefficients of models for soil-water characteristic curves. The method has proven to be powerful and reasonably efficient in identifying the optimal parameters. Mendez et al. [14] calibrated the parameters of sand hypoplastic (SH) constitutive models using GA with the recently developed open-source software GA-cal. Furthermore, they investigated the predictive limits of the SH model and, through multiobjective analysis, identified the main parameters governing the compromise between accurately predicting stresses and strains in drained monotonic tests. Macháček et al. [15] proposed an approach for the IPI of a hypoplastic soil constitutive model. Their IPI employed two different optimization algorithms, namely differential evolution (DE) and particle swarm optimization (PSO). They found that the simulations performed using the parameters

obtained from IPI exhibit good agreement with the experimental data and demonstrate improvements over the parameter sets obtained from manual calibration. While the aforementioned works suggest that the IPI method offers advantages over manual calibration, the use of relatively basic optimization algorithms (such as GA and PSO) in these studies may limit the efficiency when processing larger datasets. In recent years, the rapid development of the computer field has witnessed the emergence of numerous advanced optimization algorithms. For example, inspired by the adaptation and reproductive behavior of cuckoos, Yang and Suash [16] developed the cuckoo search algorithm (CSA). They demonstrated that CSA outperformed GA and PSO in locating global optima within certain specialized contexts [16, 17]. The successful application of CSA in various domains confirms its effectiveness in the optimization process [18], which motivates the integration of CSA into the IPI of the HCA model. One advantage of the CSA is its simplicity due to having only two control parameters. However, the original CSA also lacks efficiency when faced with complex and nonlinear optimization problems encountered in calibrating parameters of constitutive models. To further improve the performance of CSA in complex issues, many variants were developed when solving previous poor-performing optimization problems by conducting some new modifications [19]. Despite extensive efforts to enhance CSA in various aspects, its optimization capability remains limited. This study focuses on two main drawbacks, namely, poor search performance and slow convergence ability, which exist in CSA for calibrating HCA model parameters problems. The innovations and contribution of this study are as follows:

1. A novel improved CSA called ICSA is developed in the IPI of the HCA constitutive model.
2. Modifications and improvements of ICSA include the following:
 - Introducing quasi-opposition learning (QOL) to expand the search space and improve convergence speed.
 - Replacing the original search strategy with a Cauchy random walk (CRW) to enhance global search ability.
 - Introducing an ASF in the previous constant parameter in the algorithm to achieve a better balance between exploration speed and accuracy.
 - Using a dynamic inertia weight (DIW) to balance the search between global and local spaces when generating new nest positions after abandoning old ones.
3. The performance and differences in determining HCA model parameters between manual and IPI methods are compared and explained in detail.
4. The effectiveness and superiority of each improvement strategy introduced in the ICSA over the original CSA are discussed.

The main structure of this article is as follows. In Section 2, we introduced the constitutive formulas of the HCA model along with the dataset utilized for the calibration of its parameters. In Section 3, we presented a detailed analysis of the original CSA and explained the motivation behind proposing the ICSA for calibrating HCA model parameters. We outlined the application process and principle of the improvement strategies designed to enhance searchability and convergence speed. Furthermore,

we compared the performance of IPI and manual calibration in determining HCA model parameters, as well as the performance of each enhancement strategy. This assessment was grounded on a database comprising high-cyclic triaxial tests on sand, sourced from He et al. [20]. Finally, we summarized the improvement of the algorithm and discussed its superiority in determining HCA model parameters.

2 | Manual Calibration of HCA Model Parameters

2.1 | HCA Model of Sand

The HCA studied in this work was published by Niemunis et al. [5] and presented in detail by Wichtmann et al. [21]. The HCA model, proposed by Niemunis et al. [5], operates under the assumption that the strain path resulting from cyclic loading can be decomposed into an oscillating component and a trend. The strain amplitude, which is determined by the hypoplastic model, describes the oscillating part. When considering soil deformation under prolonged cyclic loading, the main objective is to predict the long-term trend of soil deformation. Consequently, an explicit-dominant approach is required to reduce computational efforts. Only a small number of cycles (i.e., the oscillating part) are implicitly calculated with numerous strain increments, while larger packages of cycles are explicitly calculated. The explicit calculation stages necessitate a constitutive formulation that incorporates packages of cycles (i.e., ΔN , where N is the number of loading cycles) as input and directly predicts the permanent strain caused by these packages, without tracing the oscillating strain path during individual cycles. This constitutive formulation is referred to as the “HCA model.” The external load is kept constant during the explicit calculation stages, treating the accumulation of permanent strain resulting from cyclic loading similarly to creep deformation in viscoplastic models.

The definitions of mean effective stress p' and deviatoric stress q used in this study are as follows:

$$p' = \text{tr}\boldsymbol{\sigma}/3 = (\sigma_1 + 2\sigma_3)/3 \quad (1)$$

$$q = \sqrt{3/2} \|\boldsymbol{\sigma}^*\| = \sigma_1 - \sigma_3 \quad (2)$$

where σ_1 and σ_3 are the major principal stress and minor principal stress, respectively; $\boldsymbol{\sigma}^*$ represents the deviatoric part of the principal stress. The work conjugated strain rates, including volumetric strain ε_v and shear strain ε_q , are stated as:

$$\varepsilon_v = \text{tr}\boldsymbol{\varepsilon} = \varepsilon_1 + 2\varepsilon_3 \quad (3)$$

$$\varepsilon_q = \sqrt{2/3} \|\boldsymbol{\varepsilon}^*\| = 2/3(\varepsilon_1 - \varepsilon_3) \quad (4)$$

where ε_1 and ε_3 are the major principal strain and minor principal strain, respectively; $\boldsymbol{\varepsilon}^*$ represents the deviatoric part of the principal strain. The expression for stress obliquity is represented by $\eta_{av} = q_{av}/p'_{av}$ or alternatively using the yield function $Y = -I_1 I_2 / I_3$ ofatsuoka and Nakai [22] as

$$\bar{Y}^{av} = \frac{Y^{av} - 9}{Y_c - 9} \quad (5)$$

$$Y^{av} = -\frac{I_1^{av} I_2^{av}}{I_3^{av}} = \frac{27(3 + \eta_{av})}{(3 + 2\eta_{av})(3 - \eta_{av})} \quad (6)$$

TABLE 1 | Summary of the functions and material constants of the HCA model.

| Functions | Constants |
|--|--------------------------|
| $f_{\text{ampl}} = \left(\frac{\varepsilon^{\text{ampl}}}{10^{-4}}\right)^{C_{\text{ampl}}}$ | C_{ampl} |
| $\dot{f}_N = \frac{C_{N1} C_{N2}}{1 + C_{N2} N} + C_{N1} C_{N3}$ | C_{N1}, C_{N2}, C_{N3} |
| $f_p = \exp[C_p (\frac{p'_{av}}{100} - 1)]$ | C_p |
| $f_Y = \exp(C_Y \bar{Y}^{av})$ | C_Y |
| $f_e = \frac{(C_e - e)^2}{1 + e} \frac{1 + e_{\text{max}}}{(C_e - e_{\text{max}})^2}$ | C_e |

$$Y_c = \frac{9 - \sin^2 \varphi_{cs}}{1 - \sin^2 \varphi_{cs}} \quad (7)$$

where φ_c denotes the critical friction angle. The inclinations of the critical state line (CSL, refer to Figure 1) are indicated as:

$$M_c = \frac{6 \sin \varphi_{cs}}{3 - \sin \varphi_{cs}} (\text{compression}); M_e = -\frac{6 \sin \varphi_{cs}}{3 + \sin \varphi_{cs}} (\text{tension}) \quad (8)$$

In all tests, the average stress σ_{av} was kept constant and the axial stress component σ_1 was cyclically varied with an amplitude q^{ampl} (see Figure 1). It is convenient to introduce the normalized form of the stress amplitude:

$$\zeta = q^{\text{ampl}} / p'_0 \quad (9)$$

where p'_0 is the initial mean effective stress. The strains under cyclic loading can be decomposed into a residual and a resilient portion denoted by the superscripts ε^{acc} and $\varepsilon^{\text{ampl}}$, respectively. The current study solely focuses on uniaxial cycles. In this scenario, the novel amplitude definition is equivalent to the conventional definition, that is, $\varepsilon^{\text{ampl}} = \varepsilon_{\text{max}} - \varepsilon_{\text{min}}$. The intensity of strain accumulation ε^{acc} is abbreviated as:

$$\varepsilon^{\text{acc}} = \sqrt{(\varepsilon_1^{\text{acc}})^2 + 2(\varepsilon_3^{\text{acc}})^2} \quad (10)$$

where $\varepsilon_1^{\text{acc}}$ and $\varepsilon_3^{\text{acc}}$ are the accumulated major principal strain and accumulated minor principal strain, respectively. Note that Equations (1)–(4) and (10) assume that the intermediate principal stress/strain (i.e., σ_2/ε_2) is equal to the minor principal stress/strain (i.e., σ_3/ε_3), implying $\sigma_2 = \sigma_3$ and $\varepsilon_2 = \varepsilon_3$. The increment of intensity of strain accumulation ε^{acc} in Equation (10) is calculated as a product of six functions:

$$\dot{\varepsilon}^{\text{acc}} = f_{\text{ampl}} \dot{f}_N f_e f_p f_Y f_\pi \quad (11)$$

each function describes a single influencing parameter (see Table 1), namely the strain amplitude $\varepsilon^{\text{ampl}}$ (function f_{ampl}), the cyclic preloading N (\dot{f}_N), void ratio e (f_e), average mean pressure p'_{av} (f_p), average stress ratio η_{av} or \bar{Y}^{av} (f_Y), and the effect of polarization changes ($f_\pi = 1$ for a constant polarization as in the case of all the test series presented in this study).

For a constant strain amplitude, the function f_N simplifies to:

$$f_N = C_{N1} [\ln(1 + C_{N2} N) + C_{N3} N] \quad (12)$$

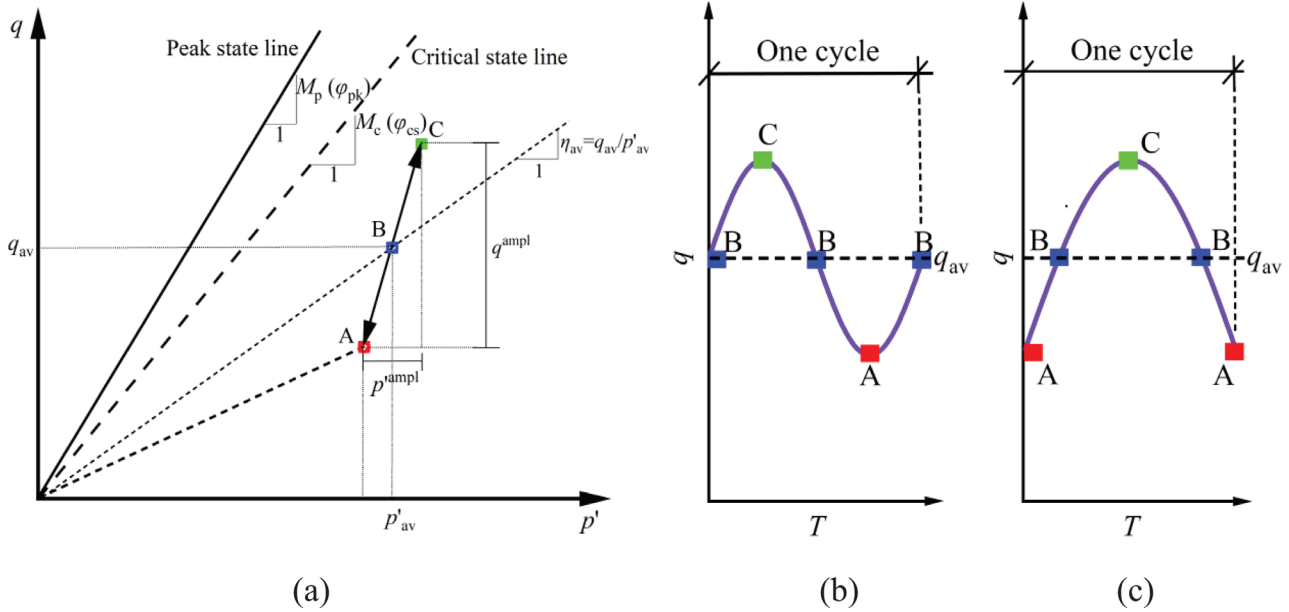


FIGURE 1 | State of stress in a cyclic triaxial test: (a) definitions for the notation; (b) sinusoidal cyclic load; (c) semi-sinusoidal cyclic load.

In the calculation of the HCA model, the stress state is kept constant and represented by the ratio $\eta_{av} = q_{av}/p'_{av}$ or \bar{Y}^{av} , where q_{av} is the average deviatoric stress and p'_{av} is the average mean effective stress corresponding to point B, as illustrated in Figure 1a. For simulating horizontal cyclic loads acting on the monopile foundation of wind turbines, a sinusoidal waveform is commonly employed for soils, as shown in Figure 1b. Conversely, a semi-sinusoidal waveform is typically utilized for soil specimens to simulate vertical cyclic loads caused by traffic loading, as depicted in Figure 1c. This is because traffic cyclic loads do not induce cyclic stress in the tensile direction. Although both forms of cyclic loading can attain the same stress states at point B (i.e., average stress states), the stress states during the cyclic loading process differ. Consequently, this discrepancy in stress states should be taken into account when calibrating the parameter within the f_{ampli} function.

2.2 | Experimental Data Under High-Cyclic Loading

The experimental data selected for analysis were obtained from tests conducted on calcareous sand subjected to high-cyclic loading [20]. This type of sand is characterized by angular-shaped grains [23, 24], poor gradation, with a mean grain size of $d_{50} = 0.14$ mm and a uniformity coefficient of $C_u = 1.5$ (see Table 2). More detailed physical properties of this type of sand can be found in He et al. [20]. The laboratory testing of this sand included both drained monotonic and cyclic triaxial tests. The cyclic triaxial tests were conducted using a semi-sinusoidal loading waveform (see Figure 1c), with cyclic stress applied only in the compression direction, for a total of 30,000 cycles. These tests aimed to investigate the long-term deformability of calcareous sand under cyclic loading induced by traffic. The frequency of cyclic loading was set at 1 Hz. The specimens tested in these experiments varied in terms of ζ , e (void ratio), p'_0 (initial mean effective stress), and η_{av} , where the four independent series

TABLE 2 | Physical properties of calcareous sand.

| Property | Value |
|-------------------------------------|----------|
| Specific gravity (G_s) | 2.75 |
| Maximum void ratio (e_{max}) | 1.347 |
| Minimum void ratio (e_{min}) | 0.91 |
| Medium particle size (d_{50}) | 0.604 mm |
| Coefficient of uniformity (C_u) | 1.8 |
| Coefficient of curvature (C_c) | 0.781 |

of cyclic stress paths are illustrated in Figure 2. The stress paths for these four series of experiments are necessarily required to determine the parameters of the HCA model.

This calcareous sand has been reported to undergo only moderate particle breakage under traffic cyclic loading [20]; therefore, it is not necessary to specifically incorporate a particle breakage function into the HCA model. Moreover, the critical state stress ratio (M_c) for this type of sand was determined to be 1.5 through monotonic drained shear tests. Detailed summary tables for the drained cyclic triaxial tests conducted on this sand can be found in Table 3.

3 | IPI for the HCA Model

The manual calibration method for the HCA model parameters was described in Wichtmann et al. [10], based on four independent series of cyclic triaxial tests shown in Figure 2. The manual parameter calibration process requires independent calibration of each function's parameters using its own independent data series and step, rather than considering interactions between different functions and parameters. Consequently, the obtained calibrated parameter values are not globally optimal. Moreover, manual calibration demands a considerable amount of fitting work and

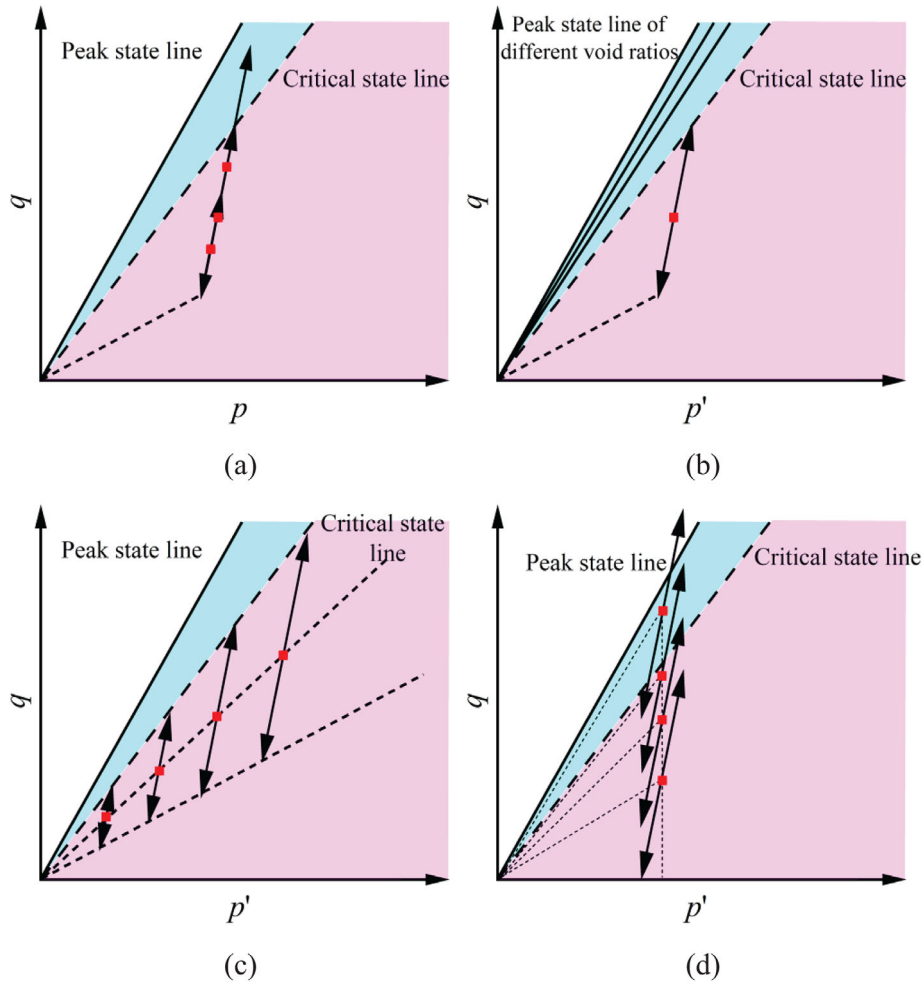


FIGURE 2 | Stress paths in tests on the influence of (a) ξ ; (b) e ; (c) p'_0 ; (d) η_{av} .

time-consuming efforts, along with a high level of expertise in fitting for the user. To overcome the limitations of manually calibrating HCA model parameters and improve the effectiveness of parameter calibration, we have proposed an automated calibration method that utilizes optimization algorithms. This method is elaborated upon in detail in the following section.

3.1 | Objective/Cost Function

For the optimization problem of determining the parameters of HCA models based on experimental or observed data, the parameters of the specific HCA model serve as the variables to be optimized. A crucial component of any optimization process is the presence of an objective or cost function that needs to be minimized by adjusting the parameters during the optimization phase. Note that the HCA model is an explicitly calculated model, and the recalculation of ϵ^{acc} in the calibration process is based on measured inputs such as average strain amplitude and void ratio. The sole goal of calibrating the HCA model parameters is to identify an optimal set of parameters that lead to the most accurate prediction of ϵ^{acc} . To ensure that the error remains unaffected by the type of test and the number of measurement points, an advanced error function can be utilized, wherein each calculation point is assigned a weight. The average difference

between the measured and simulated results is quantified using the approach similar to the weighted least squares method [25]:

$$F_{err} = \sqrt{\frac{1}{N_t} \sum_{i=1}^{N_t} \left(\frac{U_{ei} - U_{ni}}{A + BU_{ei}} \right)^2} \quad (13)$$

In the above equation, N_t is the number of test data; U_{ei} represents the i th experimental measured value, while U_{ni} corresponds to the i th value obtained from numerical calculations. A and B are constants that are used to assign varying weights to the measured points. When A is equal to zero, the points with weaker measured values are given more weight. On the other hand, when B equals zero, all points on the curve are considered to have equal weight. In alignment with the research presented in Jin and Yin [26], the values for parameters A and B were, respectively, selected as 0 and 1 in this study. The parameter set with the lowest F_{err} value can be chosen as the optimal one.

3.2 | Basic CSA

The CSA, proposed by Yang and Suash [16], has been reported to outperform GA and PSO algorithms in locating global optima within certain specialized contexts. This innovative algorithm draws inspiration from the behavior of cuckoo birds, which lay

TABLE 3 | Summary of high-cyclic triaxial test programs.

| No. | p'_0 (kPa) | ζ | Target void ratio (e_t) | $(\sigma_3/\sigma_1)_c$ | p'_{av} (kPa) | η_{av} | B value (%) | Void ratio after consolidation |
|-----|--------------|---------|-----------------------------|-------------------------|-----------------|-------------|---------------|--------------------------------|
| 1 | 40 | 0.6 | 0.998 | 0.4 | 44 | 1.18 | 97.5 | 0.997 |
| 2 | 40 | 1.0 | 0.998 | 0.4 | 46.7 | 1.29 | 98.2 | 0.997 |
| 3 | 40 | 1.8 | 0.998 | 0.4 | 52 | 1.46 | 98.1 | 0.997 |
| 4 | 70 | 0.6 | 0.998 | 0.4 | 77 | 1.18 | 98.1 | 0.997 |
| 5 | 70 | 1.0 | 0.998 | 0.4 | 81.7 | 1.29 | 97.3 | 0.996 |
| 6 | 70 | 1.8 | 0.998 | 0.4 | 91 | 1.46 | 98.1 | 0.996 |
| 7 | 100 | 0.6 | 0.998 | 0.4 | 110 | 1.18 | 99 | 0.993 |
| 8 | 100 | 1.0 | 0.998 | 0.4 | 116.7 | 1.29 | 98.2 | 0.992 |
| 9 | 100 | 1.8 | 0.998 | 0.4 | 130 | 1.46 | 98.7 | 0.992 |
| 10 | 300 | 1.0 | 0.998 | 0.4 | 350 | 1.29 | 97.6 | 0.962 |
| 11 | 300 | 0.6 | 0.998 | 0.4 | 330 | 1.18 | 97.4 | 0.961 |
| 12 | 300 | 1.8 | 0.998 | 0.4 | 390 | 1.46 | 97.1 | 0.963 |
| 13 | 40 | 0.6 | 1.14 | 0.4 | 44 | 1.18 | 97.6 | 1.135 |
| 14 | 40 | 1.0 | 1.14 | 0.4 | 46.7 | 1.29 | 97.4 | 1.133 |
| 15 | 100 | 0.6 | 1.14 | 0.4 | 110 | 1.18 | 97.6 | 1.119 |
| 16 | 100 | 1.0 | 1.14 | 0.4 | 116.7 | 1.29 | 97.9 | 1.120 |
| 17 | 300 | 0.6 | 1.14 | 0.4 | 330 | 1.18 | 98.1 | 1.082 |
| 18 | 300 | 1.0 | 1.14 | 0.4 | 350 | 1.29 | 97.2 | 1.080 |
| 19 | 40 | 0.6 | 1.26 | 0.4 | 44 | 1.18 | 97.7 | 1.252 |
| 20 | 40 | 1.0 | 1.26 | 0.4 | 46.7 | 1.29 | 97.5 | 1.256 |
| 21 | 100 | 0.6 | 1.26 | 0.4 | 110 | 1.18 | 97.8 | 1.228 |
| 22 | 100 | 1.0 | 1.26 | 0.4 | 116.7 | 1.29 | 97.6 | 1.225 |
| 23 | 300 | 0.6 | 1.26 | 0.4 | 330 | 1.18 | 97.5 | 1.178 |
| 24 | 300 | 1.0 | 1.26 | 0.4 | 350 | 1.29 | 97.4 | 1.174 |
| 25 | 300 | 1.0 | 0.998 | 1.0 | 350 | 1.29 | 97.3 | 0.960 |
| 26 | 300 | 1.0 | 0.998 | 0.286 | 350 | 1.29 | 97.1 | 0.964 |
| 27 | 300 | 1.0 | 0.998 | 0.222 | 350 | 1.29 | 97.2 | 0.967 |

Note: $(\sigma_3/\sigma_1)_c$ represents the ratio of minor principal stress (σ_3) to major principal stress (σ_1) in the consolidation stage.

their eggs in the nests of other birds, as shown in Figure 3. When the host bird realizes that the eggs do not belong to them, they have the option to either discard the eggs or abandon their own nest and construct a fresh one. The phenomenon of cuckoo egg laying and breeding served as the primary motivation for the development of this novel optimization algorithm. In the cuckoo algorithm, the position of the nest where the egg is parasitized is mapped to the solution space of the algorithm's population. The quality of the parasitized nest position is used as the fitness value of the algorithm. The basic assumptions of this algorithm are as follows:

- Each cuckoo lays only one egg at a time and randomly deposits it in a host nest. The egg represents a solution set for the problem being considered.
- Following the “survival of the fittest” rule, only a fraction of host nests with the highest quality eggs are selected to be passed on to the next generation.

- The number of host nests remains fixed. Host birds can detect a parasitic egg with a probability $P_a \in [0, 1]$. This detection can result in either the abandonment of the cuckoo egg or the abandonment of the host nest. In such instances, the host bird migrates to a new habitat and starts afresh with a new nest.

According to the above hypothesis of the spawning behavior, the formula to update the solutions in the CS algorithm is based on Lévy flight, as shown in Equation (14) below:

$$x_i^{t+1} = x_i^t + \alpha \oplus Le'vy(\lambda) (x_i^t - x_b) \quad (14)$$

where x_i^t represents the t th generation and i th bird egg; x_b represents the best solution of the t th generation; α is a step size, which is commonly set as a constant value of 1 [19, 27, 28]; the operator \oplus refers to the entry-wise multiplication; and $Le'vy(\lambda)$ denotes the random walk step size following Lévy flight. The Lévy distribution is distinguished by a sequence of immediate jumps

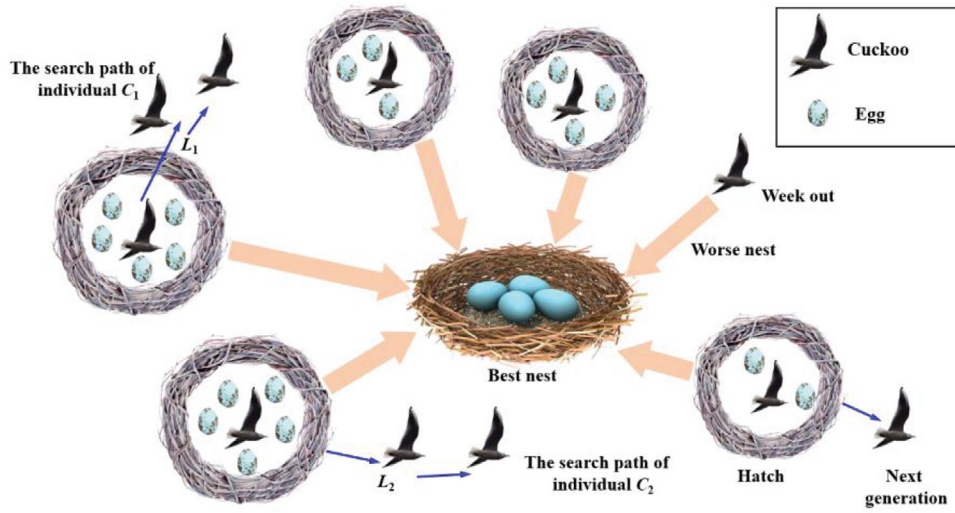


FIGURE 3 | Schematic diagram illustrating the principle of the CSA. CSA, cuckoo search algorithm.

generated by the probability density function. $Le'vy(\lambda)$ is defined as:

$$Le'vy(\beta) = \frac{u}{|v|^{\frac{1}{\beta}}} \quad (15)$$

where u and v follow a Gaussian normal distribution, with $u = Norm(0, \sigma_u^2)$ and $v = Norm(0, 1)$, and are provided by Equation (16).

$$\sigma_u^2 = \left(\frac{\Gamma(1 + \beta) \sin\left(\frac{\pi\beta}{2}\right)}{\beta \Gamma\left(\frac{1+\beta}{2}\right) * 2^{\frac{\beta-1}{2}}}\right)^{\frac{1}{\beta}} \quad (16)$$

here, β is a constant that typically ranges between 1 and 2, which is commonly considered as 1.5 [27, 29]. Γ refers to the gamma function.

After undergoing the Lévy flight and acquiring a fresh solution, a random number R within the range of 0 to 1 is generated. In the CSA, a discovery probability P_a is employed to discard certain old nests. Typically, P_a is set to 0.25 [28]. If R is less than P_a , the nest of the old bird is retained. However, if R is greater than P_a , the old nests are discarded. Subsequently, Equation (17) is employed to generate a designated number of new nests.

$$x_i^{t+1} = x_i^t + r * (x_j^t - x_k^t) \quad (17)$$

where r = random number follows a normal distribution, ranging from 0 to 1. x_j^t and x_k^t donate two different solutions randomly chosen from the generation t .

3.3 | Motivation for Enhancing CSA

When selecting an optimization algorithm, it is important to consider that the objective function of the HCA model is a highly complex and nonlinear function. This complexity is a result of the hypersensitivity of the HCA model to parameter

changes. Additionally, certain parameters in the HCA model may be interdependent. Traditional direct search and optimization algorithms relying on gradient information can lead to local optimization and premature convergence in such cases. The CSA is recognized as a remarkable optimization method due to its fast convergence and high search accuracy [17]. However, its simple structure renders it unstable when confronted with complex and nonlinear optimization problems [30, 31]. Despite extensive efforts to enhance CSA in various aspects, its optimization capability remains limited. This study aims to address two primary shortcomings of CSA when dealing with complex HCA model parameter calibration problems: inadequate search ability and slow convergence speed. To accomplish this, we introduce four modification strategies in CSA, namely the QOL, CRW, ASF, and DIW. The following sections will provide detailed explanations and demonstrations of each of the four strategies.

3.4 | Modification 1: Incorporating QOL

To enhance the convergence speed of the optimization algorithm, we introduce a novel technique called QOL, as proposed in Rahnamayan et al. [32]. The diagram illustrating the generation of opposition solutions is depicted in Figure 4. If a solution x falls within the range $[a, b]$, then its opposition solution x' based on QOL is determined as follows:

$$x' = a + b - x \quad (18)$$

The opposition solution for a solution x'_i from the D -dimensional solution p' can be derived as follows:

$$\begin{cases} p' = (x'_1, x'_2, \dots, x'_D) \\ x'_i = x_{i \min} + x_{i \max} - x_i \end{cases} \quad (19)$$

As depicted in Figure 4, it is evident that placing the feasible solution and its opposition solution on opposite sides of the search space is akin to searching two symmetric spaces simultaneously. This approach expands the search space and improves search efficiency. After generating the new solution through



FIGURE 4 | Quasi-opposition point defined in QOL. QOL, quasi-opposition learning.

QOL, it is evaluated based on its fitness with respect to the objective function. If the quality of the current solution can be improved, the newly updated solution from QOL is retained; otherwise, it is discarded. This implementation of an elite retention method further enhances the algorithm's efficiency. The QOL strategy employed in this study effectively broadens the search range of the population, explores new search spaces, and promotes population diversity. Through the utilization of an approach that generates an opposing solution and subsequently selects the superior one, QOL increases the probability of yielding individuals closer to the optimal solution. Consequently, QOL can minimize the convergence time required for problem optimization.

3.5 | Modification 2: Incorporating CRW

While the Lévy flight can explore the global space by varying the step size, it is worth considering alternative exploration methods due to the nonuniform heavy tail distribution of the Lévy flight [33]. An example of such an alternative is the CRW, which moves more stably and enables faster identification of local extremes. The Cauchy density function can be expressed as follows [34]:

$$f_{C(0,g)}(\delta) = \frac{g}{(g^2 + \delta^2)\pi} \quad (20)$$

where g is the scale parameter, typically set as 1 for the standardized distribution. The Cauchy distribution function can be expressed as:

$$y = 0.5 + \frac{1}{\pi} \arctan\left(\frac{\delta}{g}\right) \quad (21)$$

By employing Equation (21), we can derive the subsequent equation:

$$\delta = \tan(\pi(y - 0.5)) \quad (22)$$

Furthermore, we can generate a random number following the Cauchy distribution within the range of 0 to 1. This number can then be substituted into the global exploration formula, resulting in the generation of a new solution.

$$x_i^{t+1} = x_i^t + \alpha \otimes \text{Cauchy}(\lambda)(x_i^t - x_b) \quad (23)$$

The elongated tail of the Cauchy distribution allows for larger search step sizes, empowering the algorithm to escape local extremities and, thus, enhancing its search capability in the global space and ultimately improving convergence speed.

3.6 | Modification 3: Incorporating ASF

The switch parameter P_a in CSA plays a crucial role in determining the balance between exploration speed and accuracy. Previous studies have proposed various adaptive modifications for P_a to ensure a more stable search performance or accelerate the convergence speed [35, 36].

Instead of using a fixed value for P_a in original CSA, this study employs an adaptive expression for P_a based on the number of iterations. The expression is as follows:

$$P_a = 0.05 + 0.25\left(\frac{t}{T}\right)^2 \quad (24)$$

Here, t represents the current number of iterations, and T denotes the maximum number of iterations. The variation of P_a as the number of iterations progresses can be observed in Figure 5a, where P_a is observed to increase with the number of iterations. During the early stages of iteration, a small probability of P_a is utilized to discard the current bird's nest position, allowing for global search and an increase in convergence speed. As the number of iterations continues to rise, P_a keeps increasing. In the later stages of iteration, P_a experiences rapid growth. This aids the algorithm in conducting a local search as it approaches the global optimum, thereby improving the algorithm's allowed accuracy and search efficiency.

Apart from the switch parameter P_a , the step size control parameter α is another crucial parameter in CSA that has been improved in previous studies. By modifying the step size parameter α , the search step size in Equation (23) can be adaptively adjusted based on the number of iterations. The adaptive expression for α utilized in this study is as follows:

$$\alpha = 10^{-2}T \exp\left(-4\left(\frac{t}{T}\right)^{0.9}\right) \quad (25)$$

The relationship between α and the number of iterations is depicted in Figure 5b. It is clear that the value of α gradually decreases in a nonlinear fashion as the number of iterations increases. In the initial stages of optimization, a higher α results in a larger search step size, thereby expanding the search space during the early computational phase. This effectively enhances the algorithm's global optimization capability and accelerates convergence. As the number of iterations grows, the value of α decreases at a smaller rate and eventually stabilizes. This adjustment enhances the algorithm's ability to perform localized and refined searches.

3.7 | Modification 4: Incorporating DIW

Nickabadi et al. [37] proposed a DIW based on the fitness values of the best and worst individuals as follows:

$$w = \frac{f_i - f_{\min}}{f_{\max} - f_{\min}} \quad (26)$$

where f_i , f_{\max} , and f_{\min} are the fitness values of the individual i , the best individual, and the worst individual in each generation, respectively. By introducing the DIW, that is, Equation (26), in

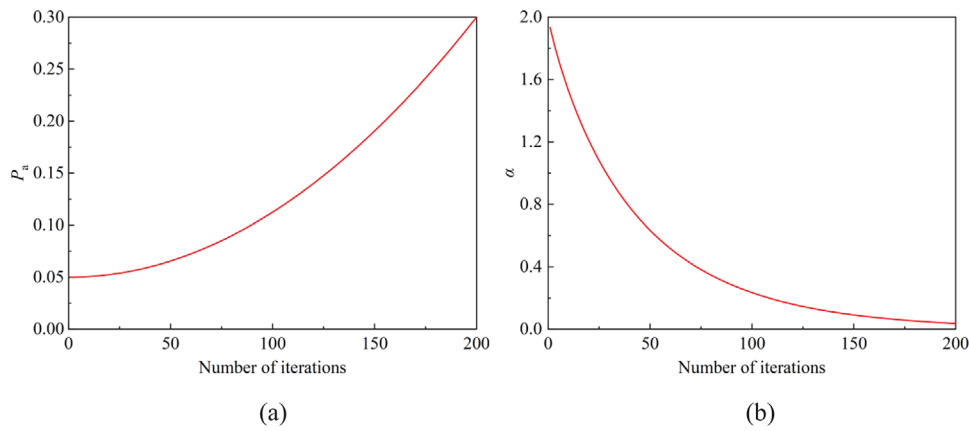


FIGURE 5 | Variation of control parameters against number of iterations: (a) P_a ; (b) α .

the step of generating new nest positions after abandoning the old nest positions (Equation 17), a more intelligent approach to generating new nests is introduced:

$$w = 1 - 0.4 \left(\frac{f_i - f_{\min}}{f_{\max} - f_{\min}} \right)^{1.5} \quad (27)$$

$$x_i^{t+1} = wx_i^t + r * (x_j^t - x_k^t) \quad (28)$$

In the CS algorithm, if the fitness difference between an individual and the best individual is significant, the inertia weight w will be smaller, thereby enhancing the local search capability. If the algorithm becomes trapped in a local optimum, the fitness difference between the individual and the best individual becomes smaller, and in this case, w increases to expand the search space. This allows the algorithm to escape from local optima and improves global search capability, thus enhancing convergence speed. Therefore, by dynamically adjusting w based on the fitness values of the nests, the algorithm can balance the search between global and local spaces and improve its ability to escape from local optima.

3.8 | Evaluating the Performance of ICSA

The application process of the improved cuckoo search algorithm (ICSA) proposed in this study is depicted in Figure 6, wherein the four additional strategies introduced in this study are highlighted in light blue. The performance of the proposed IPI method is investigated by calibrating the parameters of the HCA model using the dataset from He et al. [20], which is also used for manual calibration. This allows for a thorough examination of the differences between IPI and manual calibration of HCA model parameters. Furthermore, Figure 7 exemplifies the use of the ICSA to search for the optimal parameters of the HCA model, showcasing how each parameter progressively approaches its optimal value from an initial state. In the early stages of the search, there are significant variations in the parameters. However, as the parameters converge toward their optimal values, the variations decrease significantly during the later stages of the search. As a result, many studies adopt a fixed number of iterations as the termination condition for the search when utilizing the optimization algorithm for global optimization [31, 36]. In this study, the stop-

ping condition for each algorithm is set as reaching 200 iterations. During the search for optimal parameters using the algorithm, the ranges of the HCA model are appropriately constrained within rational boundaries that align with the acceptable and realistic parameter range of the sandy soils, as shown in Table 4.

The variation in the objective error (i.e., F_{err}) values obtained by the CSA and ICSA algorithms during the search process, as a function of the iteration number, is compared in Figure 8. To ensure fairness in the comparison, each algorithm underwent four rounds of parameter calibration tests on the HCA model due to the inherent randomness of the optimization algorithm. The optimal parameters of the HCA model discovered using intelligent algorithms correspond to the minimum objective error. As depicted in Figure 8, the search for optimal parameters of the HCA model using ICSA demonstrates a significantly quicker decrease in objective error compared to the CSA in all four tests. Furthermore, the final objective error value achieved by the ICSA is smaller. This suggests that the ICSA proposed in this study can effectively enhance both the search speed and accuracy of HCA model parameters compared to the original CSA.

To further assess the effectiveness of the four employed improvement strategies in enhancing the search capability of the CSA, the ICSA, ICSA without QOL, ICSA without CRW, ICSA without ASF, and ICSA without DIW are employed to search for the optimal model parameters of the HCA model in the dataset provided by He et al. [20], individually. The impact of each strategy on the ability to search for the optimal parameters of the HCA model is independently analyzed by excluding the strategy from the ICSA. The objective error values obtained by the five algorithms during the search process were compared in Figure 9, illustrating the variation as a function of the iteration number. Similarly, all algorithms stop searching when the number of iterations reaches 200, and all algorithms were run four times for more objective comparison. Clearly, the incorporation of all four modification strategies enhances the search performance of the CSA, as the exclusion of any strategy results in a slower reduction of objective error and a diminished search capability of the algorithm (refer to Figure 9). This highlights the necessity of employing each modification strategy in this study. Specifically, the incorporation of QOL, CRW, and DIW caused the objective error to decrease faster with the number of iterations in the early

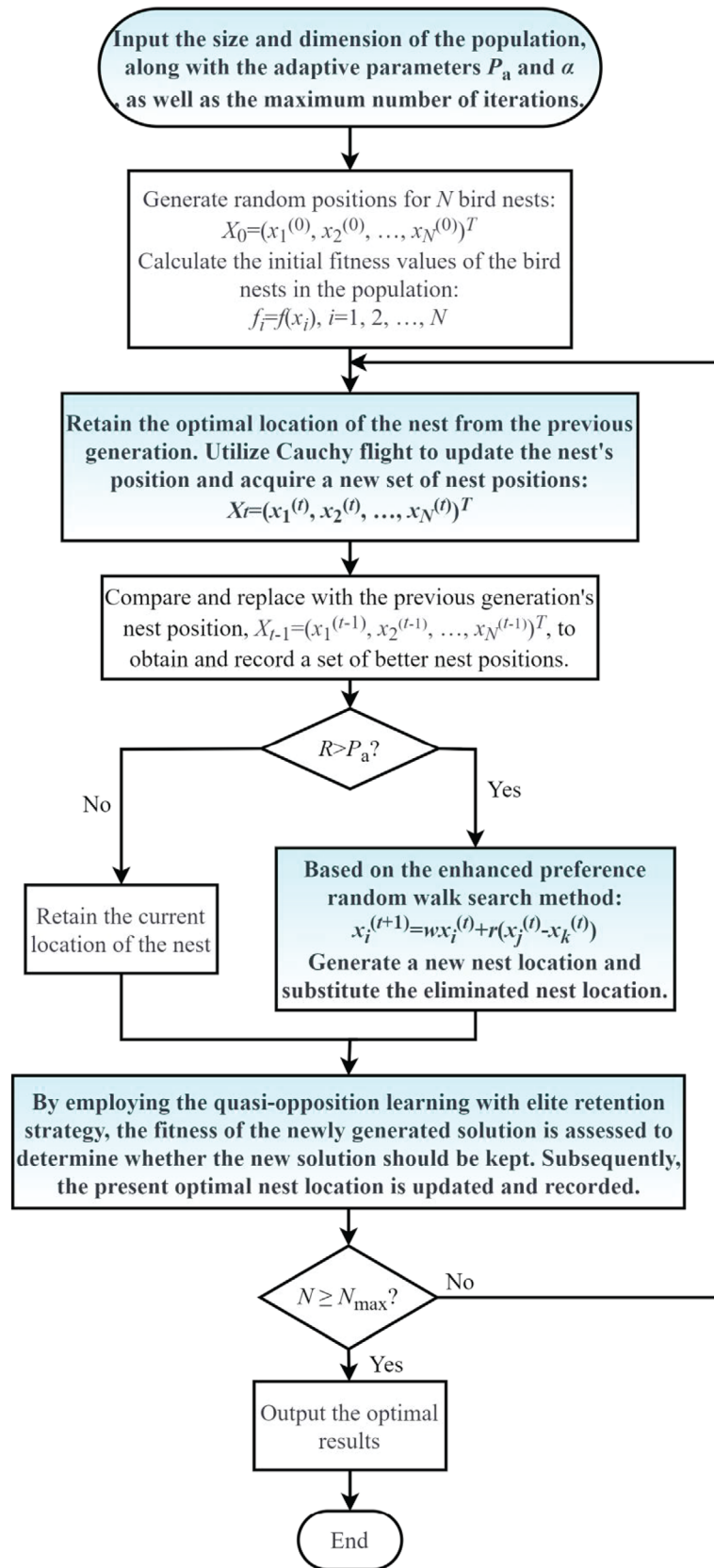


FIGURE 6 | Schematic diagram illustrating the application process of the ICSA. ICSA, improved cuckoo search algorithm.

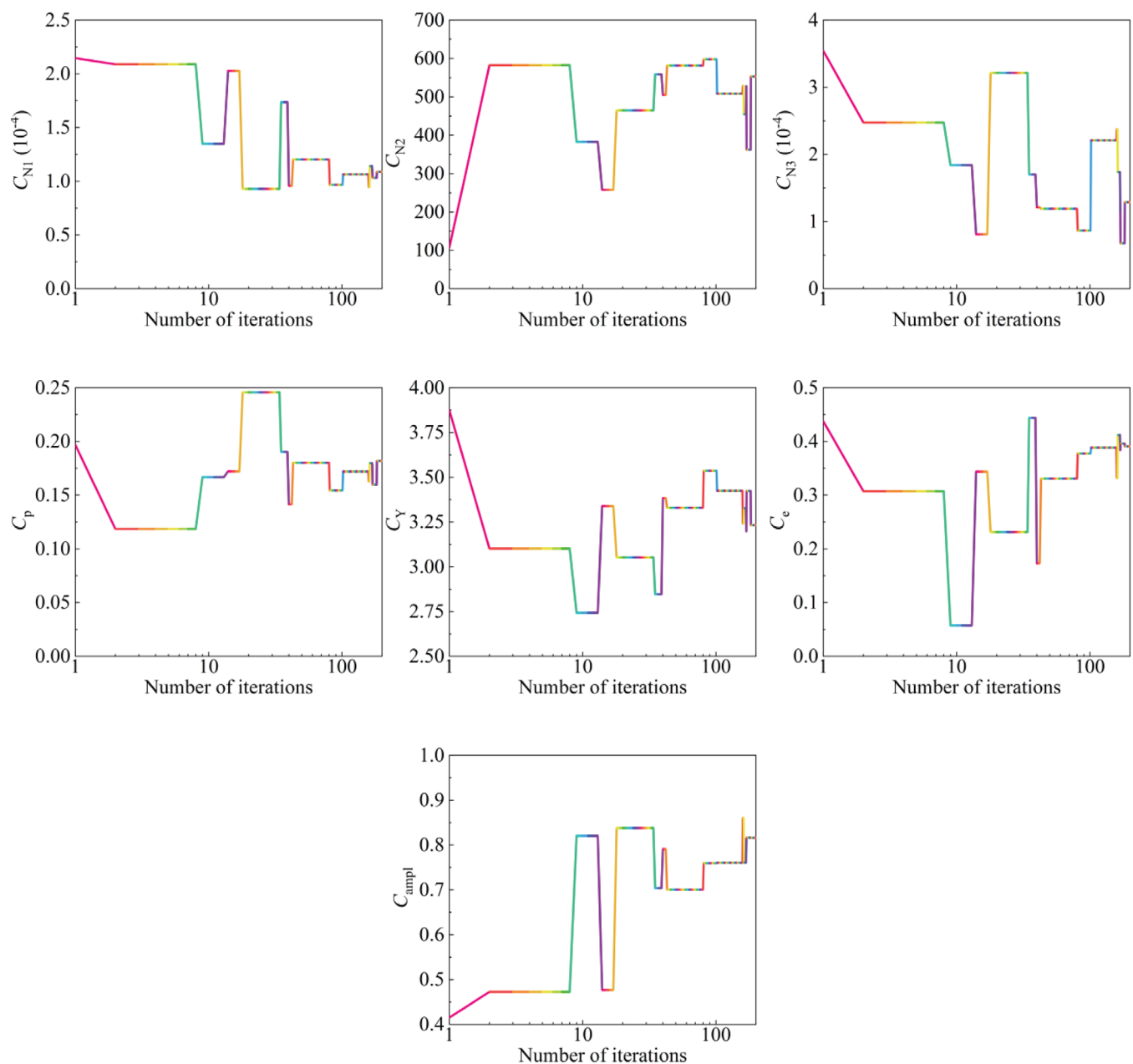


FIGURE 7 | Evolution of the HCA model parameters in the iterative process of optimization search. HCA, high-cycle accumulation.

TABLE 4 | Range of various parameters in the search process.

| | C_{N1} | C_{N2} | C_{N3} | C_{ampl} | C_e | C_p | C_Y |
|-------|-------------|----------|-----------|------------|--------|----------|--------|
| Range | [0, 1.1e-3] | [0, 600] | [0, 5e-4] | [0, 1] | [0, 5] | [0, 0.7] | [0, 3] |

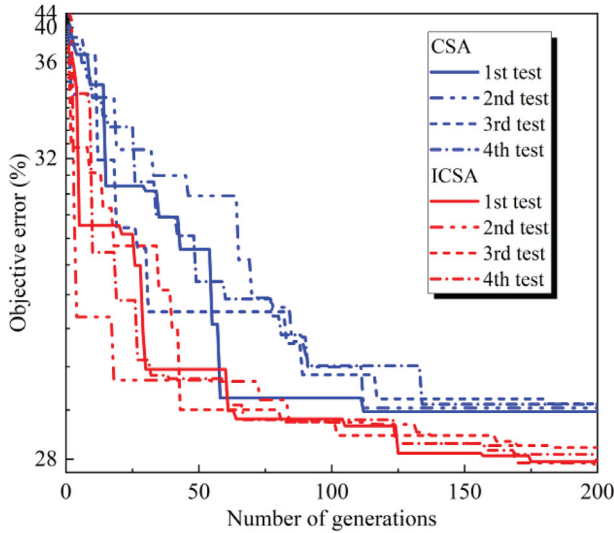
search stage, and slightly reduced the final objective error values. This indicates that the addition of QOL, CRW, and DIW significantly accelerates the convergence speed and global optimization, while the improvement in algorithm search accuracy is mild. This is because the primary focus of QOL is to increase the search space and speed of searching for global optima, and its effect on improving local optimization and final accuracy is limited. The characteristic of CRW is mainly to increase the step size in the early stage of search, while its effect on reducing the step

size in the later stage of search is mild. Therefore, its ability to increase global optimization is more significant. Although DIW can balance the speed of global search and the ability of localized search, the results in Figure 9d indicate that its ability to enhance global optimization is more beneficial. In addition, with the addition of ASF, the objective error decreases much faster with the number of iterations, and the final objective error value considerably decreases. This suggests that the inclusion of ASF can greatly improve both the speed and accuracy of the

TABLE 5 | Selected benchmark tests for evaluating the new ICSA.

| Test function | x domain | Optimum |
|--|--------------------------|--------------------|
| 1. Exponential problem: $f_1 = -(\exp(-0.5 \sum_{i=1}^n x_i^2))$ | $-1 \leq x_i \leq 1$ | $\min f(x^*) = -1$ |
| 2. Rosenbrock problem: $f_2 = \sum_{i=1}^{n-1} [100(x_{i+1} - x_i^2)^2 + (x_i - 1)^2]$ | $-30 \leq x_i \leq 30$ | $\min f(x^*) = 0$ |
| 3. Sphere function: $f_3(x) = \sum_{i=1}^n x_i^2$ | $-100 \leq x_i \leq 100$ | $\min f(x^*) = 0$ |
| 4. Ellipsoidal function: $f_4(x) = \sum_{i=1}^n (x_i + 0.5)^2$ | $-100 \leq x_i \leq 100$ | $\min f(x^*) = 0$ |

Abbreviation: ICSA, improved cuckoo search algorithm.

**FIGURE 8** | Convergence curves of the CSA and ICSA on calibrating HCA model parameters. CSA, cuckoo search algorithm; HCA, high-cycle accumulation; ICSA, improved cuckoo search algorithm.

algorithm's search. This is attributed to its expansion of the global search space in the early stage and a significant increase in the ability of local optimization in the later stage, due to adaptive changes in search step size and P_a values during the search process.

To enhance the assessment of the proposed ICSA, a selection of four mathematical functions was carefully chosen from the global optimization literature [38, 39], encompassing varying degrees of complexity and multimodality. These functions serve as benchmark tests and are listed in Table 5 alongside their theoretical optimum values. For comparative purposes, CSA was also applied to the same set of benchmark tests using identical optimization procedures. Figure 10 illustrates the progression of the minimum objective value in relation to the generation number for these benchmarks. The comparative analysis indicates a noticeable improvement in the performance of ICSA compared to CSA, particularly in terms of convergence rate and accuracy, even though the theoretical solutions for function f_2 were not achieved.

Additionally, the comparative efficiency of the CSA and ICSA algorithms is evaluated through the optimization of parameters for an equation for predicting the creep index (C_α) of clay. The creep property of soft clay is conventionally characterized by the creep index $C_\alpha = \Delta e / \Delta \log(t_s)$, where e is void ratio and t_s is time during secondary compression. Utilizing 118 clay test data

from Yin and Jin [40], an automatic parameter identification process was conducted on Equation (29) to ascertain the optimal parameters for estimating the creep coefficient of cohesive soil in correlation with water content (ω_c), plastic limit (ω_p), and plasticity index (I_p).

$$C_\alpha = (k_1 + k_2 \omega_L + k_3 I_p) \left(\frac{\omega_c}{\omega_L} \right)^{k_4 + k_5 \omega_L + k_6 I_p} \quad (29)$$

Figure 11a delineates the evolution of the objective error in relation to the generation number for the parameter identification of Equation (29). The results indicate a superior convergence rate and enhanced accuracy of the ICSA in comparison with the CSA. The outcomes of the parameter identification are detailed in Table 6, which also encompasses the R^2 and $RMSE$ values. Figure 11b,c illustrates the predictive results for the clay's creep index using model parameters identified from various algorithms. It becomes apparent that the parameters identified through the ICSA achieve more accurate predictions of the creep index than those identified from the CSA. The above-mentioned cases further substantiate the superior performance of the ICSA over the CSA in diverse scenarios.

3.9 | Predictions of ϵ^{acc}

The manual calibration of the HCA model parameters was conducted on the dataset, following the methodology outlined by Wichtmann et al. [10]. A comprehensive summary of the HCA model parameters, derived from various calibration techniques, is presented in Table 7. The HCA model is then employed to predict the ϵ^{acc} under long-term cyclic loads, utilizing model parameters derived from both manual calibration and IPI through various algorithms. To assess the predictive performance of the HCA model, the coefficient of determination (R^2) and root mean squared error ($RMSE$) values are provided in Table 7. Furthermore, Figure 12 offers a visual comparison between the measured ϵ^{acc} values and the predicted ϵ^{acc} values obtained through manual calibration, IPI with the original CSA, and IPI with the ICSA. In addition, Figure 13 illustrates the comparisons of these three calibration approaches by plotting ϵ^{acc} against N (i.e., the number of loading cycles). From Table 7 and Figures 12 and 13, it is evident that the HCA model exhibits a satisfactory ability to predict the development of ϵ^{acc} under long-term cyclic loads. This highlights its excellent applicability in analyzing long-term deformation in subgrade, railway, and pavement engineering applications. Notably, the model parameters obtained through IPI enable more precise predictions compared to manual calibration. This advantage arises from the ability of IPI methods, which rely on global optimization, to fully consider the interdependence between all

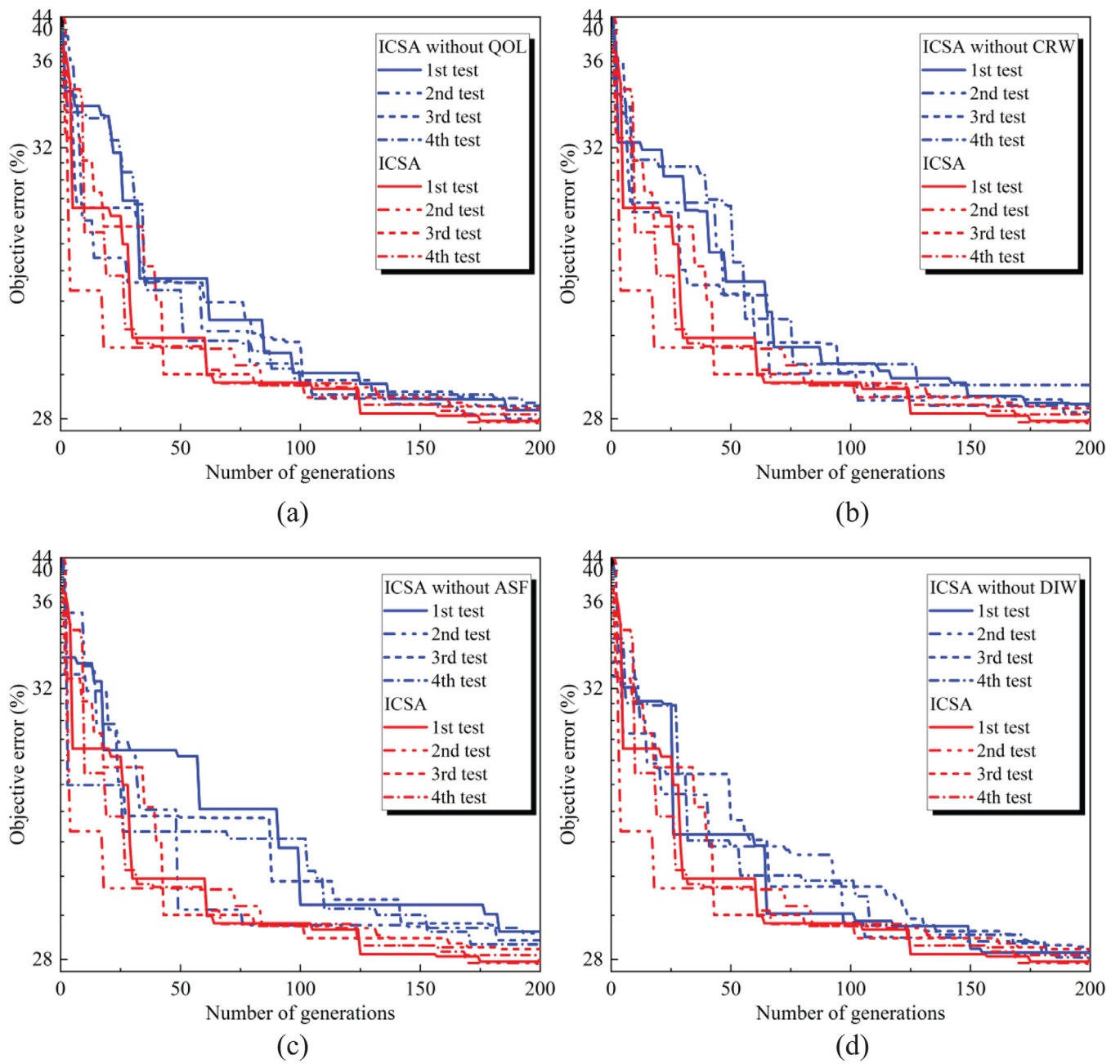


FIGURE 9 | Comparisons of convergence curves of the various algorithms on calibrating HCA model parameters: (a) ICSA without QOL; (b) ICSA without CRW; (c) ICSA without ASF; (d) ICSA without DIW. ASF, adaptive scaling factor; CRW, Cauchy random walk; ICSA, improved cuckoo search algorithm; DIQ, dynamic inertia weights; QOL, quasi-opposition learning.

TABLE 6 | Outcomes of the parameter identification for C_{α} .

| Parameters Approach | k_1 | k_2 | k_3 | k_4 | k_5 | k_6 | R^2 | RMSE |
|------------------------|---------|--------|--------|-------|-------|--------|-------|--------|
| IPI with CSA | -0.0245 | 0.0721 | 0.0087 | 0.355 | 0.707 | -0.213 | 0.83 | 0.0039 |
| IPI with ICSA | -0.0088 | 0.0099 | 0.0623 | 0.153 | 0.521 | -0.179 | 0.86 | 0.0036 |

Abbreviations: CSA, improved cuckoo search algorithm; ICSA, improved cuckoo search algorithm; RMSE, root mean squared error.

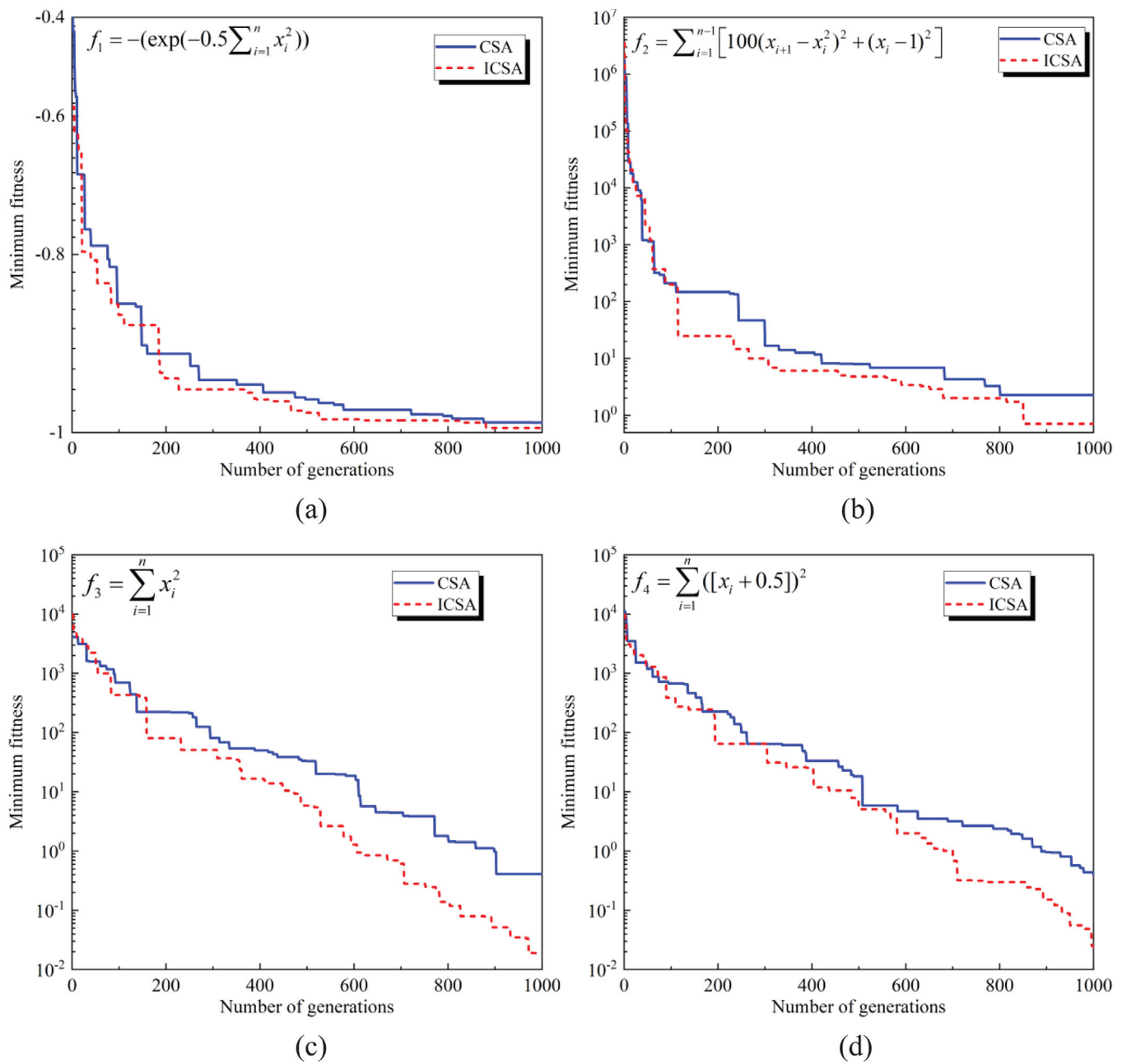


FIGURE 10 | Comparisons of optimized results on benchmark tests for CSA and ICSA: (a) f_1 ; (b) f_2 ; (c) f_3 ; (d) f_4 . CSA, cuckoo search algorithm; ICSA, improved cuckoo search algorithm.

TABLE 7 | Summary of calibration and prediction results for different approaches.

| Parameters Approach | C_{N1} (10^{-4}) | C_{N2} | C_{N3} (10^{-4}) | C_{ampl} | C_e | C_p | C_Y | R^2 | RMSE |
|--------------------------------------|---|----------------------------|---|-------------------------------------|-------------------------|-------------------------|-------------------------|-------------------------|-------------|
| Manual calibration | 1.09 | 318.6 | 1.28 | 1.1 | 0.55 | 0.17 | 3.72 | 0.87 | 0.00909 |
| IPI with CSA | 0.99 | 294.5 | 0.63 | 0.79 | 0.24 | 0.18 | 3.37 | 0.91 | 0.00746 |
| IPI with ICSA | 1.09 | 552.9 | 1.29 | 0.82 | 0.39 | 0.18 | 3.23 | 0.94 | 0.00608 |

Abbreviations: CSA, improved cuckoo search algorithm; ICSA, improved cuckoo search algorithm; RMSE, root mean squared error.

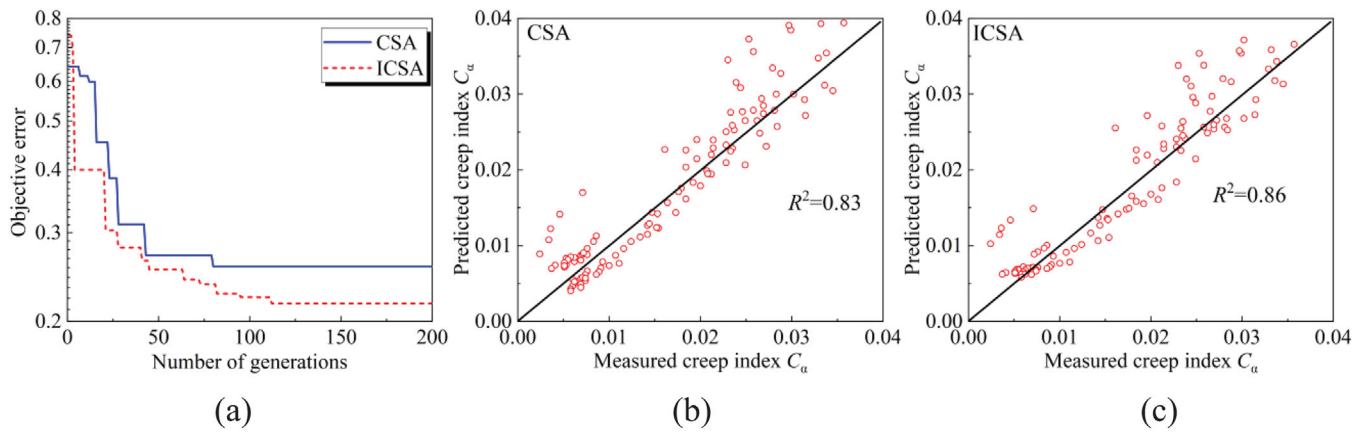


FIGURE 11 | Comparisons of optimized results on creep index C_α for CSA and ICSA: (a) convergence curves; (b) prediction based on CSA; (c) prediction based on ICSA.

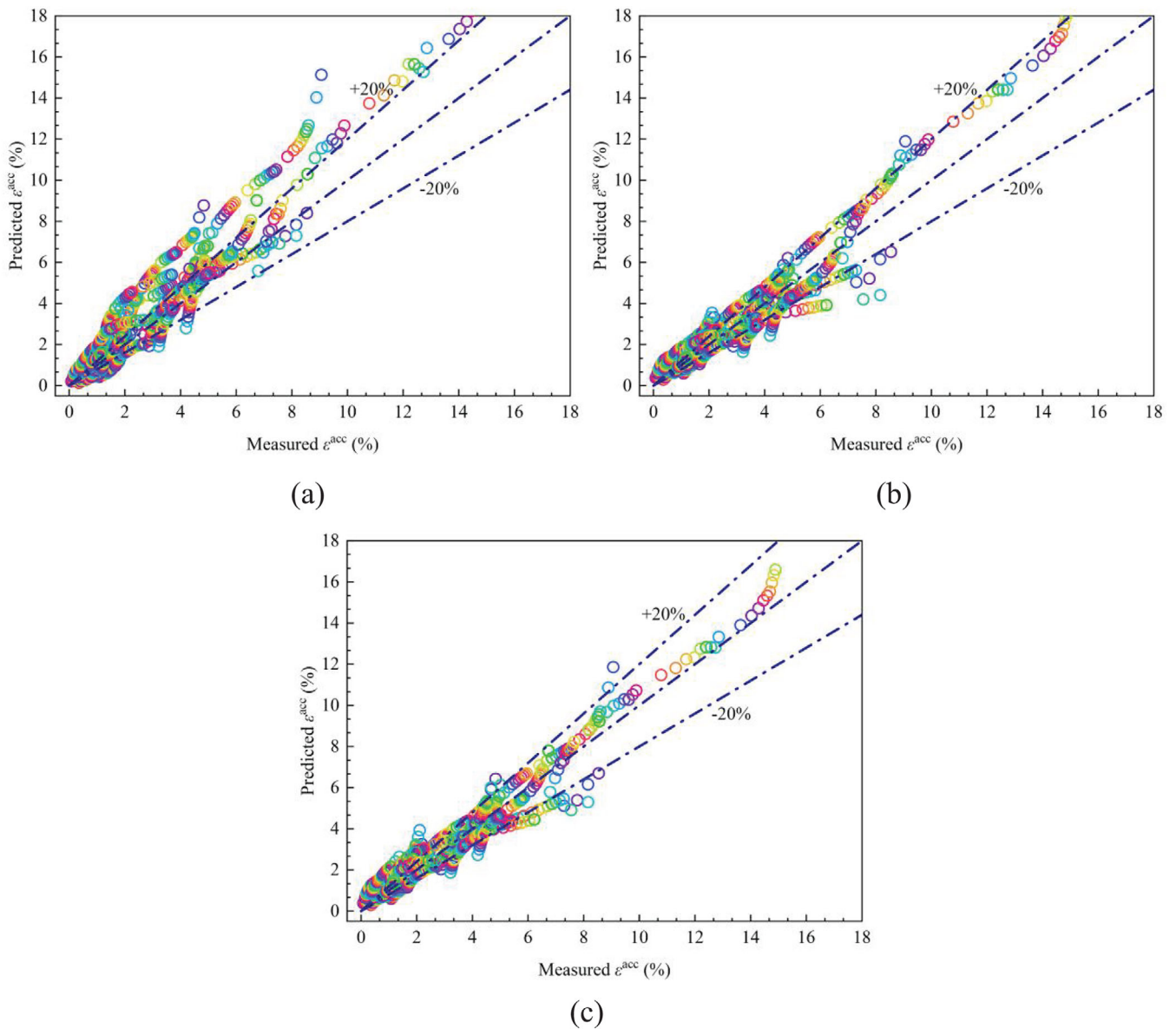


FIGURE 12 | Comparison between the measured ϵ^{acc} values and the predicted ϵ^{acc} values obtained through: (a) Manual calibration; (b) IPI with the original CSA; (c) IPI with the ICSA.

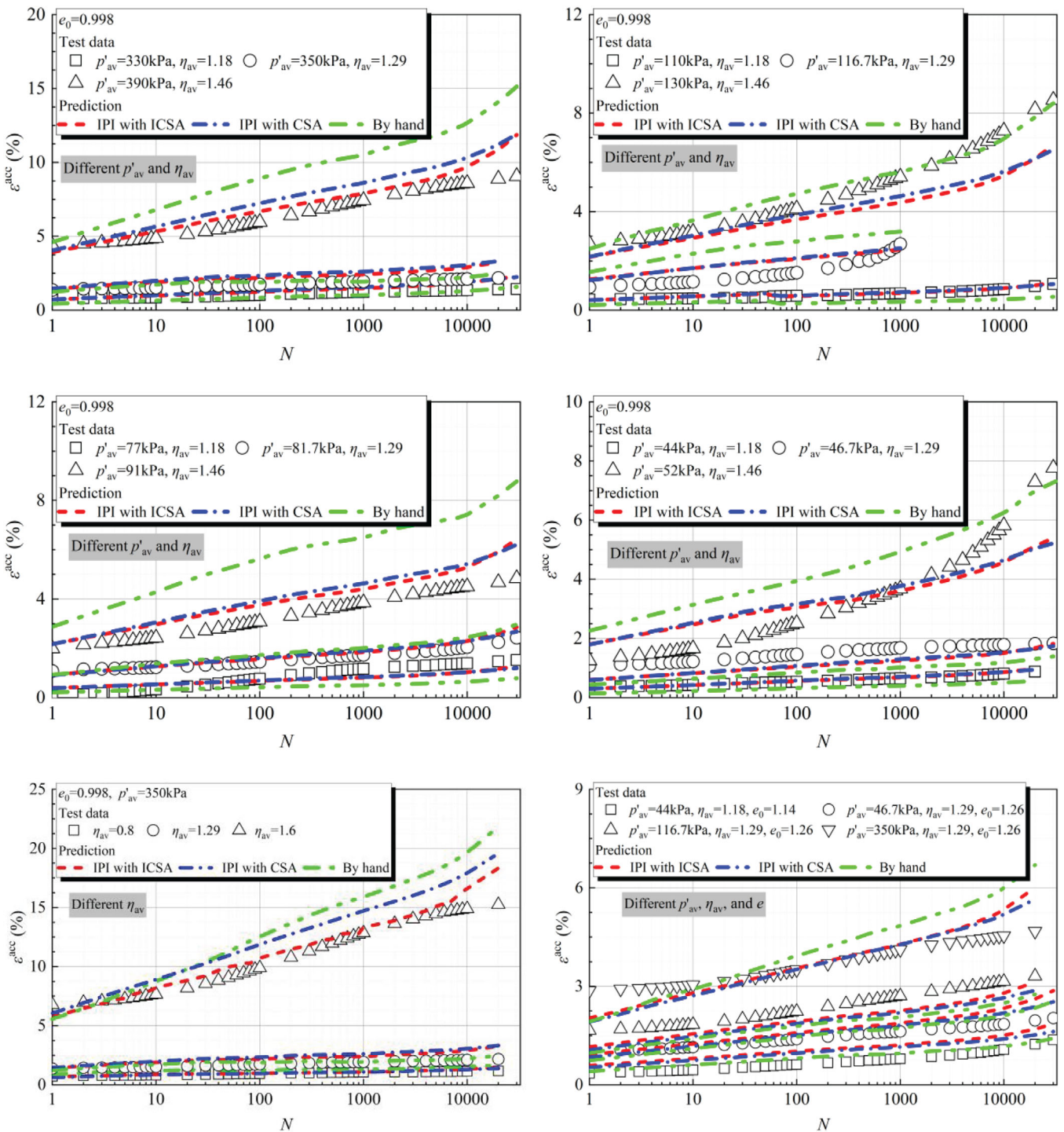


FIGURE 13 | Comparisons of observed and predicted ε^{acc} against N .

data and parameters. In contrast to manual calibration, IPI not only saves time but also achieves higher accuracy. Therefore, IPI methods facilitate the improved application of the HCA model in practical engineering tasks, such as predicting foundation settlement or facilitating structural design. Additionally, Table 7 and Figures 12 and 13 reveal that the use of the ICSA in the IPI method yields higher prediction accuracy compared to the CSA. This emphasizes the advantage of the proposed ICSA in calibrating the HCA model, ultimately enhancing the precision of engineering design and analysis.

4 | Conclusions

An ICSA was developed and utilized for the IPI of HCA model parameters. The improved CSA incorporated four novel strategies to enhance the search ability and convergence speed when engaged in finding the optimal HCA model parameters. Firstly, QOL was employed to expand the search space. Secondly, the original search strategy was replaced with CRW to further improve the global search ability. Thirdly, an ASF was introduced in the two control parameters of CSA to achieve a better balance

between exploration speed and accuracy. Lastly, the DIW was introduced in the step of generating new nest positions after abandoning the old nest positions, to balance the search between global and local spaces and improve its ability to escape from local optima.

The effectiveness and superiority of ICSA-based IPI in addressing practical problems, as well as the performance of each enhancement strategy, were assessed by identifying parameters of the HCA model based on high-cyclic triaxial tests on sand. The manual parameter calibration was also conducted for comparison. The parameters derived from different approaches were used to recalculate the intensity of the accumulation strain. The results demonstrated that the ICSA-based IPI approach could more efficiently determine the parameters of the HCA model and improve the accuracy compared to the manual calibration approach. Additionally, the ICSA considerably improved both the accuracy and search speed in identifying the parameters of the HCA model compared to the original CSA. It was observed that the strategies of QOL, CRW, and DIW could improve global search ability and convergence speed, while slightly increasing search accuracy. The strategy of ASF was found to considerably increase both global search speed and the accuracy of local search. Moreover, the recalculation of accumulated strain using the parameters derived from ICSA-based IPI yielded the best agreement with the measured results, surpassing the parameters derived from manual calibration and CSA-based IPI.

The HCA model could effectively capture the long-term deformation behavior of sand, and the intelligent identification using the ICSA made the model application easy and efficient. In the future, efforts will be made to further enhance this algorithm's performance on various constitutive models, such as the hypoplastic model, and to address practical problems in a general and efficient manner.

Acknowledgments

This research was financially supported by the Research Grants Council (RGC) of Hong Kong Special Administrative Region Government (HKSARG) of China (Grant No.: 15220221, 15229223, 15227923), the Research Centre for Resources Engineering towards Carbon Neutrality (RCRE) of The Hong Kong Polytechnic University (Grant No.: 1-BBEM) and the open fund project of Key Laboratory of Safe Construction and Intelligent Maintenance for Urban Shield Tunnels of Zhejiang Province (Grant No. ZUCC-UST-22-01).

Conflicts of Interest

The authors declare no conflicts of interest.

Data Availability Statement

The data that support the findings of this study are available from the corresponding author upon reasonable request.

References

1. S.-H. He, Z. Ding, T.-D. Xia, et al., "Long-Term Behaviour and Degradation of Calcareous Sand Under Cyclic Loading," *Engineering Geology* 276 (2020): 105756.

2. C. Pasten, H. Shin, and J. C. Santamarina, "Long-Term Foundation Response to Repetitive Loading," *Journal of Geotechnical and Geoenvironmental* 140, no. 4 (2014): 04013036.
3. C. Karg, S. François, W. Haegeman, and G. Degrande, "Elasto-Plastic Long-Term Behavior of Granular Soils: Modelling and Experimental Validation," *Soil Dynamics and Earthquake Engineering* 30, no. 8 (2010): 635–646.
4. M. Abdelkrim, P. De Buhan, and G. Bonnet, "A General Method for Calculating the Traffic Load-Induced Residual Settlement of a Platform, Based on a Structural Analysis Approach," *Soils and Foundations* 46, no. 4 (2006): 401–414.
5. A. Niemunis, T. Wichtmann, and T. Triantafyllidis, "A High-Cycle Accumulation Model for Sand," *Computers and Geotechnics* 32, no. 4 (2005): 245–263.
6. A. S. J. Suiker and R. de Borst, "A Numerical Model for the Cyclic Deterioration of Railway Tracks," *International Journal for Numerical Methods in Engineering* 57, no. 4 (2003): 441–470.
7. J. Macháček, T. Wichtmann, H. Zachert, and T. Triantafyllidis, "Long-Term Settlements of a Ship Lock: Measurements Vs. FE-Prediction Using a High Cycle Accumulation Model," *Computers and Geotechnics* 97 (2018): 222–232.
8. P. Staubach and T. Wichtmann, "Long-Term Deformations of Monopile Foundations for Offshore Wind Turbines Studied With a High-Cycle Accumulation Model," *Computers and Geotechnics* 124 (2020): 103553.
9. H. Zachert, T. Wichtmann, P. Kudella, and T. Triantafyllidis, "Inspection of a High-Cycle Accumulation Model for Sand Based on Recalculations of a Full-Scale Test on a Gravity Base Foundation for Offshore Wind Turbines," *Computers and Geotechnics* 126 (2020): 103727.
10. T. Wichtmann, A. Niemunis, and T. Triantafyllidis, "Improved Simplified Calibration Procedure for a High-Cycle Accumulation Model," *Soil Dynamics and Earthquake Engineering* 70 (2015): 118–132.
11. G. Gioda and G. Maier, "Direct Search Solution of an Inverse Problem in Elastoplasticity: Identification of Cohesion, Friction Angle and in Situ Stress by Pressure Tunnel Tests," *International Journal for Numerical Methods in Engineering* 15, no. 12 (1980): 1823–1848.
12. S. Pal, G. Wije Wathugala, and S. Kundu, "Calibration of a Constitutive Model Using Genetic Algorithms," *Computers and Geotechnics* 19, no. 4 (1996): 325–348.
13. D. M. Pedroso and D. J. Williams, "Automatic Calibration of Soil–Water Characteristic Curves Using Genetic Algorithms," *Computers and Geotechnics* 38, no. 3 (2011): 330–340.
14. F. J. Mendez, M. A. Mendez, N. Sciarra, and A. Pasculli, "Multi-Objective Analysis of the Sand Hypoplasticity Model Calibration," *Acta Geotechnica* 19 (2024): 4241–4254.
15. J. Macháček, P. Staubach, C. E. G. Tavera, T. Wichtmann, and H. Zachert, "On the Automatic Parameter Calibration of a Hypoplastic Soil Model," *Acta Geotechnica* 17, no. 11 (2022): 5253–5273.
16. X. S. Yang and D. Suash, "Cuckoo Search Via Lévy Flights," 2009 World Congress on Nature & Biologically Inspired Computing, (Coimbatore, India: NaBIC, 2009), 210–214.
17. X.-S. Yang and S. Deb, "Engineering Optimisation by Cuckoo Search," *International Journal of Mathematical Modelling and Numerical Optimisation* 1 (2010): 330.
18. M. Shehab, A. T. Khader, and M. A. Al-Betar, "A Survey on Applications and Variants of the Cuckoo Search Algorithm," *Applied Soft Computing* 61 (2017): 1041–1059.
19. X. Li, X. Guo, H. Tang, R. Wu, and J. Liu, "An Improved Cuckoo Search Algorithm for the Hybrid Flow-Shop Scheduling Problem in Sand Casting Enterprises Considering Batch Processing," *Computers & Industrial Engineering* 176 (2023): 108921.

20. S.-H. He, Z. Ding, Y. Sun, W.-Y. Chen, and T.-D. Xia, "Cumulative Deformations and Particle Breakage in Calcareous Sand Subjected to Drained High-Cyclic Loading: Experimental Investigation," *Soil Dynamics and Earthquake Engineering* 161 (2022): 107417.
21. T. Wichtmann, A. Niemunis, and T. Triantafyllidis, "Strain Accumulation in Sand Due to Cyclic Loading: Drained Triaxial Tests," *Soil Dynamics and Earthquake Engineering* 25, no. 12 (2005): 967–979.
22. H. Matsuoka and T. Nakai, "A New Failure Criterion for Soils in Three-Dimensional Stresses (UN Nouveau Critere De Rupture Pour Des Sols Soumis A Des Contraintes Tridimensionnelles)," In *Proceedings of the IUTAM Symposium on Deformation and Failure of Granular Materials*, Vermeer PA, Luger HJ (eds.), Delft, 1982: 253–263.
23. S.-H. He, Z. Ding, M. Goudarzy, Y. Sun, and Z.-Y. Yin, "Effect of Variable Confining Pressure on the Long-Term Cyclic Behaviour of Calcareous Sand: Experimental Observation and Microstructural Interpretation," *Canadian Geotechnical Journal* 61, no. 2 (2024): 311–327.
24. S.-H. He, M. Goudarzy, Z. Ding, and Y. Sun, "Strength, Deformation, and Particle Breakage Behavior of Calcareous Sand: Role of Anisotropic Consolidation," *Journal of Geotechnical and Geoenvironmental Engineering* 149, no. 3 (2023): 04023002.
25. S. Levasseur, Y. Malécot, M. Boulon, and E. Flavigny, "Soil Parameter Identification Using a Genetic Algorithm," *International Journal for Numerical and Analytical Methods in Geomechanics* 32, no. 2 (2008): 189–213.
26. Y.-F. Jin and Z.-Y. Yin, "Enhancement of Backtracking Search Algorithm for Identifying Soil Parameters," *International Journal for Numerical and Analytical Methods in Geomechanics* 44, no. 9 (2020): 1239–1261.
27. S. Gao, Y. Gao, Y. Zhang, and T. Li, "Adaptive Cuckoo Algorithm With Multiple Search Strategies," *Applied Soft Computing* 106 (2021): 107181.
28. P. Ong and Z. Zainuddin, "An Optimized Wavelet Neural Networks Using Cuckoo Search Algorithm for Function Approximation and Chaotic Time Series Prediction," *Decision Analytics Journal* 6 (2023): 100188.
29. M. Liang, L. Wang, L. Wang, and Y. Zhong, "A Hypervolume-Based Cuckoo Search Algorithm With Enhanced Diversity and Adaptive Scaling Factor," *Applied Soft Computing* 151 (2024): 111073.
30. H. Malik, A. Iqbal, P. Joshi, S. Agrawal, and F. I. Bakhsh, *Metaheuristic and Evolutionary Computation: Algorithms and Applications* (Dordrecht, the Netherlands: Springer, 2021).
31. W. Luo and X. Yu, "Reinforcement Learning-Based Modified Cuckoo Search Algorithm for Economic Dispatch Problems," *Knowledge-Based Systems* 257 (2022): 109844.
32. S. Rahnamayan, H. R. Tizhoosh, and M. M. A. Salama, "Quasi-Optimizational Differential Evolution," *2007 IEEE Congress on Evolutionary Computation* (Singapore: IEEE, 2007), 2229–2236.
33. H. Sun, X. Xie, T. Sun, and W. Pang, "Improved Cuckoo Search Algorithm for Solving Antiaircraft Weapon-Target Optimal Assignment Model," *Acta Armamentarii* 40, no. 1 (2019): 189–197.
34. R. Salgotra, U. Singh, G. Singh, S. Singh, and A. H. Gandomi, "Application of Mutation Operators to Salp Swarm Algorithm," *Expert Systems With Applications* 169 (2021): 114368.
35. E. Valian, S. Tavakoli, S. Mohanna, and A. Haghi, "Improved Cuckoo Search for Reliability Optimization Problems," *Computers & Industrial Engineering* 64, no. 1 (2013): 459–468.
36. X. Ou, M. Wu, Y. Pu, B. Tu, G. Zhang, and Z. Xu, "Cuckoo Search Algorithm With Fuzzy Logic and Gauss–Cauchy for Minimizing Localization Error of WSN," *Applied Soft Computing* 125 (2022): 109211.
37. A. Nickabadi, M. M. Ebadzadeh, and R. Safabakhsh, "A Novel Particle Swarm Optimization Algorithm With Adaptive Inertia Weight," *Applied Soft Computing* 11, no. 4 (2011): 3658–3670.
38. Z.-Y. Yin, Y.-F. Jin, S.-L. Shen, and H.-W. Huang, "An Efficient Optimization Method for Identifying Parameters of Soft Structured Clay by an Enhanced Genetic Algorithm and Elastic–Viscoplastic Model," *Acta Geotechnica* 12, no. 4 (2017): 849–867.
39. K. Deep and M. Thakur, "A New Mutation Operator for Real Coded Genetic Algorithms," *Applied Mathematics and Computation* 193, no. 1 (2007): 211–230.
40. Z.-Y. Yin and Y.-F. Jin, *Practice of Optimisation Theory in Geotechnical Engineering* (Dordrecht, the Netherlands: Springer, 2019).